Author's personal copy

Journal of Applied Geophysics 69 (2009) 51–58

Contents lists available at ScienceDirect

Journal of Applied Geophysics

journal homepage: www.elsevier.com/locate/jappgeo

DEM generation using ERS–ENVISAT interferometry

Urs Wegmüller [a,*], Maurizio Santoro [a], Charles Werner [a], Tazio Strozzi [a], Andreas Wiesmann [a], Wolfgang Lengert [b,1]

[a] Gamma Remote Sensing AG, Worbstrasse 225, CH-3073 Gümligen, Switzerland
[b] ESA-ESRIN, Via Galileo Galilei, 00044 Frascati, Italy

ARTICLE INFO

Article history:
Received 26 May 2008
Accepted 3 April 2009

Keywords:
ERS–ENVISAT interferometry
DEM generation
SAR interferometry

ABSTRACT

Space-borne SAR interferometry is one possible method for the generation of digital elevation models (DEMs). The sensitivity of this technique depends strongly on system parameters as the time interval between the observations used and the spatial baseline. Longer time intervals are less suited because of temporal decorrelation of the signal. Longer spatial baselines result in an increased height sensitivity. ERS-2 and ENVISAT ASAR operate in identical orbits at slightly different sensor frequencies with ASAR preceding ERS-2 by 28 min. This configuration offers a unique opportunity to study and apply ERS–ENVISAT interferometry. ERS-2–ENVISAT ASAR IS2 VV-polarization interferograms are characterized by a short 28 min repeat-pass interval and a long 1.5–2.5 km baseline. Given the long baseline and short time interval ERS–ENVISAT interferometry has a good potential for the generation of precise DEMs in relatively flat areas. The idea to use ERS–ENVISAT interferometry for DEM generation is not new, nevertheless, very few adequate data sets were identified and analyzed in the past. Now, thanks to a recent dedicated ERS-2–ENVISAT Tandem mission of ESA many well suited data sets became available. In this paper the ERS–ENVISAT interferometry methodology is described, its feasibility is demonstrated by presenting ERS–ENVISAT interferometry DEMs over several sites, and its potential is assessed.

© 2009 Elsevier B.V. All rights reserved.

1. Introduction

A variety of techniques to generate DEMs exist. One method is space-borne Synthetic Aperture Radar (SAR) interferometry. For an introduction to SAR interferometry it is referred to Rosen et al. (2000) and Bamler and Hartl (1998). Between the launch of ERS-2 in July 1995 and the end of ERS-1 in early 2000, the European Space Agency (ESA) operated the two European Remote Sensing (ERS) satellites in the so-called ERS-1/2 Tandem mission, acquiring interferometric SAR data with a 1 day interval. The short interferometric interval is of interest as it reduces temporal decorrelation of the signal. High coherence is required for the reliable interpretation of the interferometric phase as done in the derivation of interferometric DEMs.

In 2002 ESA launched the ENVISAT satellite with the Advanced SAR (ASAR). While the SAR sensors onboard the ERS satellites were operated in a single mode, at VV-polarization and incidence angles between about 20° and 26°, the ASAR is a multi-mode instrument which can be operated at different polarizations, incidence angles (swaths), and spatial resolutions. One of the ASAR modes, namely IS2 at VV-polarization, corresponds closely to the ERS SAR mode, except for the slightly different sensor frequency used. Furthermore, ENVISAT is operated in the same orbits as ERS-2, preceding ERS-2 by approximately 28 min. A unique opportunity offered by these two similar SAR instruments operated in the same orbital configuration is ERS–ENVISAT interferometry. The almost simultaneous acquisition of SAR images by the ERS-2 and the ENVISAT satellites (in ERS-like mode, i.e. ASAR IS2 VV-polarization) allows the generation of a new type of interferogram characterized by a short 28 min repeat-pass interval. However, because of the slightly different sensor frequency, cross-interferograms show coherence only under particular conditions. Besides the requirement concerning an at least partial Doppler spectra overlap, only at perpendicular baselines of approximately 2 km can the look-angle effect on the reflectivity spectrum compensate for the carrier frequency difference effect. Given the large baseline and short time interval ERS–ENVISAT interferometry is expected to have a good potential for the generation of precise digital elevation models (DEMs) in relatively flat areas. There is interest in such DEMs e.g. in coastal zones with low relief, river plains, and wetlands, in particular at high latitudes where the SRTM DEM (Rabus et al., 2003) is not available.

In spite of more than 7 years time overlap of the ERS-2 and ENVISAT missions relatively few investigations concerning ERS–ENVISAT interferometry were published so far. Long before the launch of ENVISAT Monti Guarnieri and Prati (2000) recognized already the possibility of using cross-interferograms. Examples of ERS–ENVISAT interferograms were then presented by Arnaud et al. (2003), Colesanti

* Corresponding author. Tel.: +41 31 9517005; fax: +41 31 9517008.
E-mail addresses: wegmuller@gamma-rs.ch (U. Wegmüller), santoro@gamma-rs.ch (M. Santoro), cw@gamma-rs.ch (C. Werner), strozzi@gamma-rs.ch (T. Strozzi), wiesmann@gamma-rs.ch (A. Wiesmann), Wolfgang.Lengert@esa.int (W. Lengert).
URL: http://www.gamma-rs.ch (U. Wegmüller).
[1] Tel.: +39 06 941801; fax: +39 06 94180280.

0926-9851/$ – see front matter © 2009 Elsevier B.V. All rights reserved.
doi:10.1016/j.jappgeo.2009.04.002

Author's personal copy

et al. (2003), Hong and Won (2005, 2006), Wegmüller et al. (2005), and Santoro et al. (2007). But all together the examples shown cover only a handful of test sites, including one pair each over Las Vegas, Paris, New Orleans, Prague, and the Wadden Sea and few pairs over Korea. The reasons for this low number of examples investigated are that only a limited number of adequate pairs exist because of the baseline and Doppler requirements and the difficulty in identifying adequate pairs in the data catalogues. The few examples presented were enough, though, to demonstrate the feasibility of ERS–ENVISAT interferometry and to indicate that further investigation would be of high interest. In order to specifically collect data suited for ERS–ENVISAT interferometry ESA conducted between 27 September 2007 and 12 February 2008 a dedicated ERS-2–ENVISAT Tandem Mission. The mission characteristics are described in section 2. In section 3 we introduce the cross-sensor interferometry methodology and data processing aspects. Then in section 4 ERS–ENVISAT interferometry DEMs over several sites are presented and the potential of the technique is discussed, followed by conclusions and outlook in section 5.

2. ERS-2–ENVISAT Tandem mission

Since its launch in 2002, ENVISAT has been operated in the same orbit as ERS-2, preceding ERS-2 by 28 min. Long baselines between the two sensors occurred only occasionally because both sensors were kept in narrow orbital tubes. Nevertheless, the availability of ERS-2 and ENVISAT provides a unique opportunity to acquire interferometric pairs with a very short time interval but a long 2 km baseline. To support further investigation of ERS–ENVISAT interferometry ESA decided in 2007 to operate ERS-2 and ENVISAT for a certain time period as a constellation to acquire many additional pairs suited for cross-sensor interferometry. In the following, this dedicated operation is called the ERS-2–ENVISAT Tandem mission. To maximise the number of acquisitions of 28-minute SAR pairs suitable for cross-sensor interferometry, the two satellites were piloted in carefully controlled orbits during the ERS-2–ENVISAT InSAR Campaign between 27 September 2007 and 12 February 2008. During this period, the nominal perpendicular baseline for mid to high northern latitudes was 2 km with ERS-2 observing the area at a slightly higher incidence angle than ASAR, to compensate for the slight difference in the carrier frequencies between the two instruments. ERS-2 SAR (in the following shortened ERS-2) and ENVISAT ASAR IS2 Mode sensor characteristics are listed in Table 1. The main difference is the 31 MHz difference in the carrier frequency.

A major limitation to ERS–ENVISAT interferometry is the often non-overlapping Doppler spectra of the two sensors. While the SAR instrument onboard ERS-2 continues to work well, there is also ample hydrazine for continued operation and preventative measures have been implemented to compensate for ageing of the power system. After 2000 the attitude control degraded because of failures of several gyroscopes. Since January 2001 ERS-2 operates in the so-called zero-gyro mode. This caused very significant yaw variations with Doppler Centroid deviations

Table 1
ERS-2 and ENVISAT ASAR IS2 mode characteristics.

Parameter	ERS-2 SAR	ENVISATA SAR IS2 VV
SAR_center_frequency	5.300 GHz	5.331 GHz
Polarization	VV	VV
Nominal_antenna_look_angle	20.350°	20.138°
Orbits	35-day repeat cycles	Same as ERS-2, ~28′ ahead of ERS-2
Pulse_repetition_frequency	1679.9 Hz	1652.42 Hz
Azimuth_pixel_spacing	3.97 m	4.04 m
Doppler spectra	Nominal Doppler spectra overlap strongly	
Chirp_bandwidth	1.555e+07 Hz	1.600e+07 Hz
ADC_sampling_frequency	1.896e+07 Hz	1.921e+07 Hz
Range_pixel_spacing	7.90 m	7.80 m

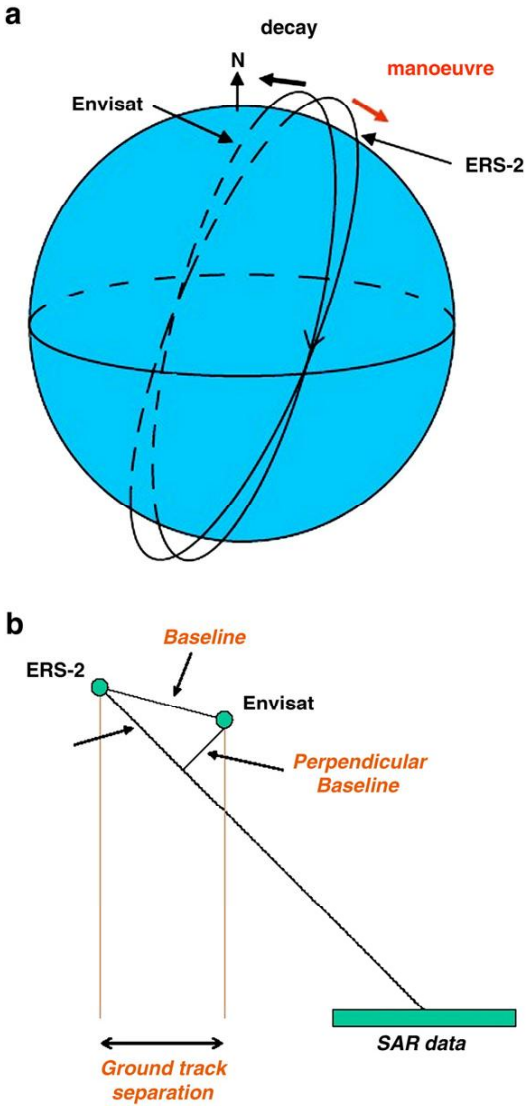


Fig. 1. Image a shows the orbital geometry with large baselines at higher northern latitudes. Image b shows the interferometric imaging geometry. ENVISAT ASAR has a 31 Mhz higher carrier frequency than ERS-2. The incidence angle effect compensates the carrier frequencey effect on the reflectivity spetrum for a perpendicular baseline $B_\perp$ of approx. 2.0 km. The sign of the baseline is such that ENVISAT sees the area under a steeper incidence angle. ERS-2 and ENVISAT carry right looking sensors, so seen in flight direction, the ENVISAT orbit has to be the right than the ERS-2 orbit.

from the nominal value of several KHz. Nevertheless, the implementation of several corrective measures strongly reduced this pointing difficulty. In the so-called Yaw Control Monitoring (YCM), yaw measurements are derived in near-real time. The objective is to automatically correct instrument attitude if necessary to maintain yaw values within ±2°. Between 2001 and August 2003 this was done using Wave Mode data. Currently, Scatterometer data are used for this purpose, which is more accurate. Furthermore, information on the actual Doppler Centroid values is becoming available in the catalogues, so that at present a significant fraction of the acquired data can again be used, also for interferometry. For more detailed information on the ERS-2 performance and discussion of corrective measures it is referred to Miranda et al. (2004) and Meadows et al. (2007).

The objectives of the dedicated InSAR campaign were to explore new interferometry applications such as the derivation of very accurate low relief digital elevation models and velocity maps of fast

Author's personal copy

Table 2
Interferometric characteristics of ERS-2–ENVISAT pairs used to derive DEMs.

Site	Date	$B_\perp$ [m]	dDC [Hz]
East Frisia	18-Oct-2007	2021	391
Po Delta	7-Nov-2007	2002	817
Netherlands	24-Oct-2007	2017	602
Seeland	15-Oct-2007	1890	237

$B_\perp$ stands for the perpendicular baseline component, dDC for the difference between the Doppler Centroid of the ERS-2 and the ENVISAT ASAR scenes.

moving Arctic glaciers and to improve the general understanding of interferometry and coherence.

Owing to the necessary configuration of the orbits of ERS-2 and ENVISAT, the InSAR Campaign favoured northern hemisphere mid and high-latitude areas by acquiring suitable data between 60°N on the ascending limb and 30°N on the descending limb, thus providing opportunities for ERS-2–ENVISAT interferometry over Arctic Polar regions, Europe, North America and most of Asia.

3. ERS–ENVISAT interferometry methodology and data processing

3.1. Theory

A SAR observes a surface area under a specific incidence angle. Given this incidence angle, the radar carrier or center frequency, and the chirp bandwidth, a certain part of the reflectivity spectrum of the surface is measured. Changes to the incidence angle or to the radar frequency cause changes of the range reflectivity spectrum. To obtain coherence between two acquisitions, the reflectivity spectra of the two signals being interfered have to overlap. For two acquisitions acquired at the same frequency this means that the incidence angle difference needs to be small. For incidence angle differences corresponding to baselines larger than the so-called critical baseline the reflectivity spectra do not overlap anymore, resulting in complete decorrelation of the signal over distributed targets. In the case of acquisitions at different frequencies the effect of the frequency on the reflectivity spectrum has also to be considered. In fact, there exists a condition under which the incidence angle effect is exactly compensated by the radar frequency effect. For a given frequency difference (f_2-f_1) the perpendicular baseline component $B_\perp$ for which the two effects compensate each other is approximately (Monti Guarnieri and Prati, 2000, Colesanti et al., 2003, Santoro et al., 2007)

$$B_\perp \cong \frac{(f_2 - f_1)\cdot r_1 \tan(\theta - \alpha)}{f_1} \quad (1)$$

In the case of the 31 MHz carrier frequency difference between ERS-2 and ENVISAT ASAR perpendicular baselines of approximately 2 km and the look-angle effect on the reflectivity spectrum compensate for a flat surface. The condition is however sensitive to the local incidence angle, $(\theta-\alpha)$. Fig. 1 illustrates the orbital configuration and the acquisition geometry with a 2 km baseline that compensates the frequency difference effect. The effect of having a perpendicular baseline just close to the optimal value ensures only partial overlap of the reflectivity spectra. As long as the overlap is significant high coherence can be maintained by common band filtering (Gatelli et al., 1994), i.e. by only considering the overlapping part of the reflectivity spectra. Because of the spatial variation of the slope angle α this common band filtering should be done in a spatially adaptive manner.

Another constraint to finding coherence in an ERS–ENVISAT interferometric pair is that overlapping Doppler spectra of the images acquired by the two sensors are required. Again, in the case of only partial overlap, the coherence is optimized by common band filtering, this time of the azimuth spectra.

Apart from the range common band filtering that needs to be adapted considering the center frequency difference the interferogram generation for a cross-sensor interferogram is identical to that of a single sensor interferogram.

In a complex-valued focused SAR image the phase corresponds to a sum of a term related to the return path of the signal and a term related to the arrangement of the scatterers in the resolution cell. For cells with many distributed scatterers this second part results in speckle with a spatially random phase in the interval $[-\pi, \pi]$. However, images acquired from almost the identical observation angle

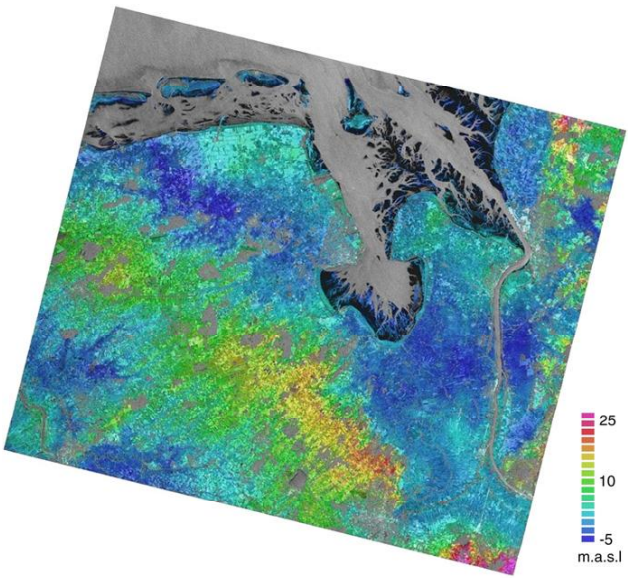


Fig. 2. East Frisia, Germany, ERS–ENVISAT interferometry DEM (18-Oct-2007, dt 28′, $B_\perp$ 2021 m, dDC 391 Hz). The average backscattering coefficient is used for the image brightness. The DEM size is approximately 85 km×75 km.

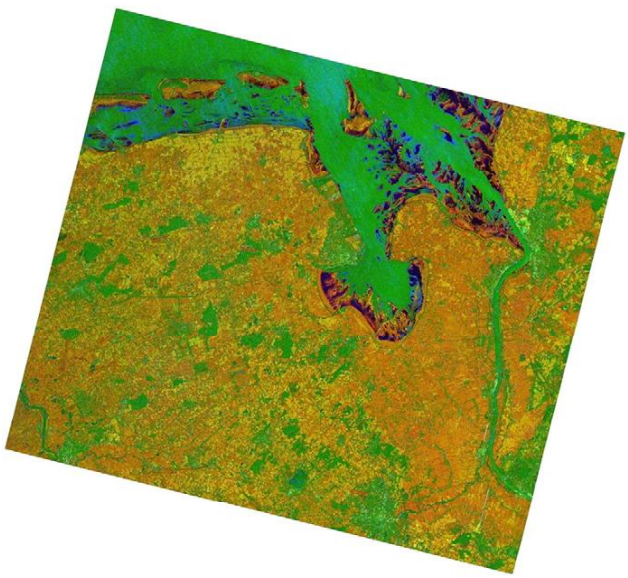


Fig. 3. Geocoded ERS–ENVISAT coherence product over East Frisia, Germany, which is an RGB composite of R: coherence, G: average backscattering, and B: backscatter change (ratio).

Author's personal copy

have almost identical speckle. Under such conditions the phase difference ϕ can be expressed as

$$\phi = -\left(\frac{4\pi f_2}{c}\left|r_2\right| - \frac{4\pi f_1}{c}\left|r_1\right|\right) \quad (2)$$

where f_1 and f_2 are the radar center frequencies, r_1 and r_2 are the slant ranges of the two scenes. Notice, that there is a significant range phase ramp even in the case of a zero baseline related to the different center frequencies

$$\frac{d\phi}{dr} = \frac{4\pi(f_{ASAR} - f_{ERS})}{c} = 1.3\frac{\text{rad}}{\text{m}} \quad (3)$$

in the ERS–ENVISAT case this results in a phase ramp of 1.3 rad per meter slant range, or more than a full phase cycle per range pixel spacing.

For $f_1 = f_2$ well known equations describe the dependence of the interferometric phase on orbit geometry, scene topography, line-of-sight surface displacements, and atmospheric path delay

$$\phi = \phi_{orb} + \frac{4\pi}{\lambda}\frac{B_\perp}{r\cdot\sin\theta}h + \frac{4\pi}{\lambda}r_{disp} + \phi_{path} + \phi_{noise} \quad (4)$$

with an orbital phase term ϕ_{orb}, the wavelength, λ, and the baseline component perpendicular to the look vector, $B_\perp$, the incidence angle, θ, the slant range, r, the slant range difference, r_{disp}, the path delay term ϕ_{path}, and a phase noise (or decorrelation) term ϕ_{noise}. In the case of slightly different frequencies $f_1 \neq f_2$ Eq. (4) can still be used as a good approximation with only minor adaptations. The orbital phase, this is the interferometric phase observed of the flat ellipsoid, is calculated using (2) with r_1 and r_2 being the slant ranges to the flat ellipsoid. This term also contains the strong range phase ramp of (3). Apart from this the only difference is that an average wavelength is used

$$\lambda = \frac{2c}{f_1 + f_2} \quad (5)$$

The phase to height sensitivity of ERS–ENVISAT interferograms at mid-swath is

$$\frac{d\phi}{dh} = \frac{4\pi}{0.056439\text{m}\cdot 852'000\text{m}\cdot\sin 23^\circ}B_\perp = 0.0006688\frac{\text{rad}}{\text{m}^2}\cdot B_\perp \quad (6)$$

For a 2.0 km baseline this corresponds to 1.34 rad/m corresponding to a height ambiguity, defined as the height per topographic phase cycle, of 4.70 m. This height ambiguity is only 10% of the one of an ERS-1/2 Tandem pair with a 200 m baseline.

Rodríguez and Martin (1992) presented an analytic expression for the Cramer–Rao bound on the phase variance. For large enough look numbers, N, used in the estimation of the interferometric phase and non-zero coherence γ the phase standard deviation can be estimated from

$$\text{stdev}(\phi_{noise}) = \frac{\sqrt{1-\gamma^2}}{2N\cdot\gamma} \quad (7)$$

Even for an intermediate coherence (0.5) and 5 looks the phase standard deviation is low (0.173 rad), corresponding for a 2 km baseline to a height sensitivity of 0.13 m.

Concerning the displacement phase term, the main difference to single sensor interferograms is that the displacement is considered over the short 28 minute time interval. Even a 1 cm/day deformation rate causes over the 28 minute interval only a deformation phase of 0.044 rad. Consequently, over this short interval most surfaces can be considered stable. The exception to this are fast moving glaciers where movement in the dm/day to m/day range occur. For most other surfaces, the deformation phase term can be ignored.

Changes in the atmospheric conditions (mainly water vapour) cause a variable path delay. Spatial heterogeneity of ϕ_{path} results in the so-called atmospheric distortions, one of the main error sources in repeat-pass SAR interferometry. In the case of non-turbulent atmospheric conditions, the spatial variation of the path delay should not be very strong. The related phase term observed in the interferogram corresponds to the difference between the path delays of the two individual acquisitions. Under non-turbulent conditions the variation in this path delay over 28 min is typically quite low and spatially rather smooth. In this case typical height errors expected are below 1 m. In the case, of a turbulent atmosphere, wind will move around the path delay heterogeneities even within 28 min. Strong and more complex atmospheric phase distortions can occur, even for 28 minute pairs, so that we expect height errors up to a few meter.

3.2. Data processing

For each image pair, interferometric processing consisted of co-registration at sub-pixel level, spatially adaptive azimuth and range common band filtering considering the baseline and frequency offset as well as the azimuth spectra effects, generation of the interferogram and removal of topographic phase. In some cases a constant height, in other cases the SRTM DEM (Rabus et al., 2003) was used as height reference. Using the SRTM DEM is quite attractive as the resulting differential interferometric phases become quite smooth even over large areas which facilitates phase unwrapping. On the other hand it is important to be aware of the quite high phase noise introduced by the topographic phase simulated from the SRTM heights. As we use the SRTM DEM also in the discussion of the derived ERS–ENVISAT DEMs we include in the following a short discussion on the SRTM DEM.

SRTM stands for Shuttle Radar Topographic Mission. The main product of this mission was a DEM covering most of the land area between $\pm 60°$ latitude. This DEM was generated using single-pass interferometry. While the DEM was generated using a 1-arc-second pixel spacing the data set that is widely available is at the reduced 3-arc-seconds resolution. For our work we did not use the original SRTM DEM, but a conditioned data set. The conditioning included the replacement of missing values through interpolation and by transformation and oversampling of the data set to the actual map geometry used in the different cases. For more detailed information on the SRTM DEM quality we refer to Rodríquez et al. (2006), who assessed the quality in much detail. For Eurasia Rodriquez et al., 2006 conclude that the SRTM height error (90%) is 6.2 m, including errors at different spatial scales. In our work using ERS-ENVISAT interferometry we consider mainly DEMs in areas with minimal relief. At the high phase to height sensitivity of 2 km baseline interferograms the 6.2 m height error of the SRTM DEM corresponds to more than one full phase cycle, therefore it is expected that the SRTM DEM may look quite noisy at this scale. For this reason we started either from a constant reference height or from strongly spatially filtered SRTM heights, this to avoid the SRTM quality influencing the quality of the results.

For processing, multi-look factors of 1 and 5 in range and azimuth respectively were used to decrease noise, resulting in $20\times 20\ \text{m}^2$ pixel size. All images were finally geocoded to $20\times 20\ \text{m}^2$ pixel size using an oversampled version of the SRTM DEM. All images shown are in cartographic projection.

In previous investigations done before the dedicated ERS-2–ENVISAT Tandem mission, a critical issue of ERS–ENVISAT interferometry was that the image pair suitable for interferometry typically presented only a rather small common band in range or azimuth. The effects of the small common band and non-perfect common band filtering were low coherence and degraded spatial resolution (see Santoro et al., 2007, Hong and Won, 2005). The newer examples from

Author's personal copy

the dedicated ERS-2–ENVISAT Tandem mission show excellent range spectra overlaps across the entire scene.

4. Results

In a first part of the results section, the focus is on demonstrating with examples over different sites that data of the dedicated ERS-2–ENVISAT Tandem mission are well suited for DEM generation over relatively flat areas. The previously shown ERS–ENVISAT interferometry results were in fact mostly differential interferograms and not really DEMs; steps as phase unwrapping and phase to height conversion was often not addressed. Furthermore, the result could sometimes only be derived for a part of the scene because of partly insufficient baseline or Doppler conditions, and the spatial resolution was reduced because most baselines used were significantly smaller than 2 km. Using data from the ERS-2–ENVISAT Tandem mission on the other hand had the advantage that the baselines were often ideal. Consequently, DEMs could be retrieved more easily, at better resolution, higher quality, and for full frames.

In a second part, we will then focus on demonstrating the potential of these large baseline DEMs. For this, the DEMs will be considered more locally and will be compared with the widely available SRTM DEM.

4.1. ERS–ENVISAT interferometry DEM examples

ERS–ENVISAT interferometry pairs from the dedicated ERS-2–ENVISAT Tandem mission were used to derive DEMs over various relatively flat sites. The baseline and Doppler Centroid conditions for the examples shown are listed in Table 2. Large area DEM results are shown in Figs. 2–6.

East Frisia is famous for the Wadden Sea, an extensive tidal mud flats area that stretches along the North Sea coasts of the Netherlands, Germany, and Denmark. The islands in the Wadden Sea are called the Frisian Islands. The Wadden Sea is important for the rich fauna, avifauna, and flora. Today, a great part of the Wadden Sea is protected, in Germany this is the Wadden Sea National Park. Through the influences of the sea and winds the landscape is constantly changing. Furthermore, parts of the mainland are threatened by flood risk from the rivers Weser and Elbe. Accurate topographic information in this low relief area is consequently of high importance for various reasons. The ERS–ENVISAT interferometry DEM is shown in Fig. 2. The terrain heights vary between about 5 m below sea level and 25 m above sea level. Heights are also obtained for some tidal flats. This is of interest as these tend to change more rapidly than the mainland. The interferogram coherence is shown in Fig. 3. The coherence relates to the land cover, with low coherence found over water and forest. For built up areas the coherence is also low because of geometric decorrelation related to the 2 km baseline. This is in contrast with ERS-1/2 Tandem coherence which is typically acquired with short baselines. For a more in-depth discussion of the ERS–ENVISAT interferometry coherence it is referred to Santoro et al., 2007.

The city of Venice, its surrounding lagoon and the Po River Delta in Italy represent a unique coastal environment. Low-lying agricultural farmland was reclaimed during the last century and is usually characterized by soils rich in organic matter. Since a large portion of

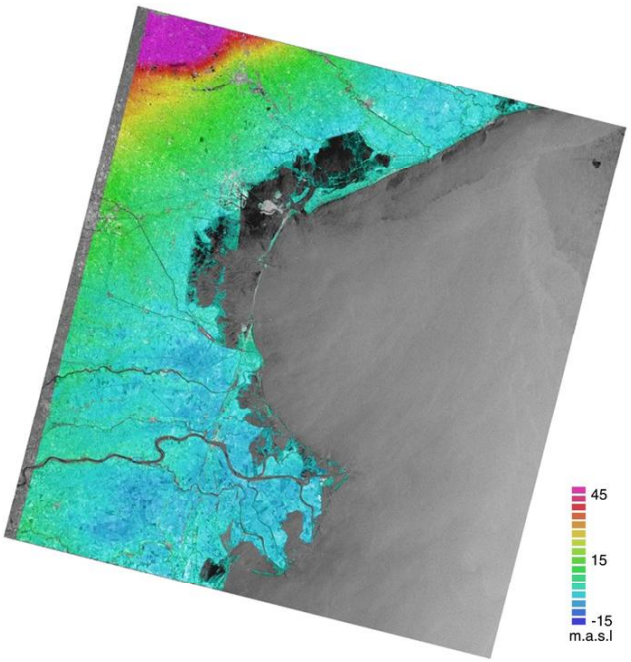


Fig. 4. Po Delta, Italy, ERS-ENVISAT cross-interferometry DEM (7-Nov-2007, dt 28′, $B_\perp$ 2002 m, dDC 817 Hz). The average backscattering coefficient is used for the image brightness. The DEM size is approximately 100 km × 100 km.

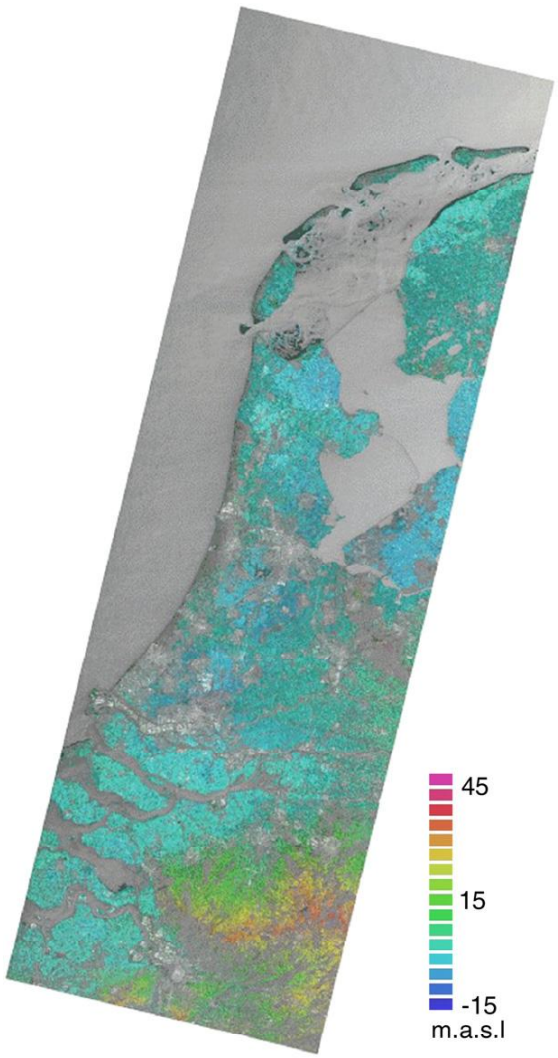


Fig. 5. Western Netherlands ERS–ENVISAT interferometry DEM (24-Oct-2007, dt 28′, $B_\perp$ 2017 m, dDC 602 Hz). The average backscattering coefficient is used for the image brightness. The DEM size is approximately 100 km × 300 km.

Author's personal copy

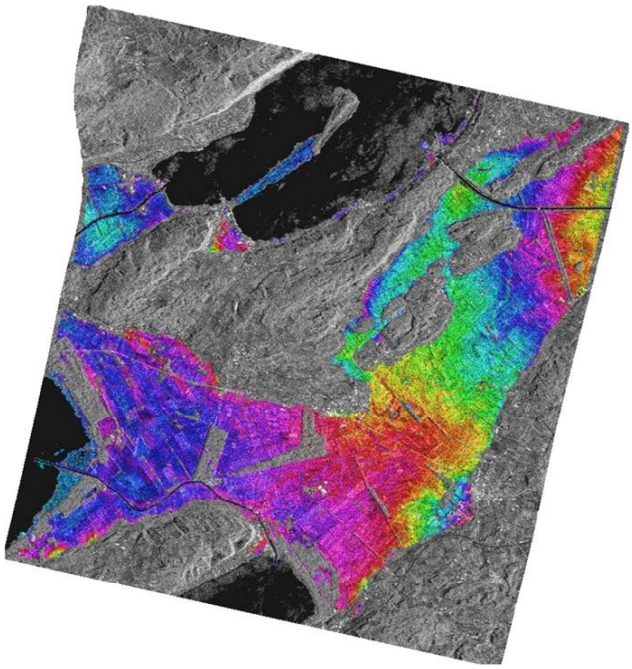


Fig. 6. Seeland, Switzerland, ERS–ENVISAT interferometry DEM (15-Oct-2007, dt 28′, $B_\perp$ 1890 m, dD 237 Hz). The average backscattering coefficient is used for the image brightness. The DEM size is 17.6 km × 18.6 km. A cyclic color scale (10 m height per color cycle) is used to highlight local height variations.

these territories presently lie below the mean sea level (down to −4 m.a.s.l.), land subsidence has represented one of the most serious environmental problems and has been the subject of many studies also using differential SAR interferometry (Teatini et al., 2005, 2007). Terrain height information is also of particular interest for the large agriculture areas and the lagoon system in relation to the environmental vulnerability and the geological hazard. An overview of the resulting ERS–ENVISAT DEM is shown in Fig. 4. For much of the area the terrain heights are close to the sea level, the exception to this is the area to the north toward the Alps.

Along the coasts of the Netherlands the terrain is quite flat. An ERS–ENVISAT interferometry DEM over the western part of the Netherlands is shown in Fig. 5. In this case 3 consecutive frames were concatenated into a single large scene. The approximate resulting image size is 300 km × 100 km. Interest in highly accurate DEMs is evident considering the flat coastal zone, areas below sea level, and a high potential flood risk.

The Seeland region is an area located between the lakes of Neuchatel, Bienne, and Morat in the western part of Switzerland. Fig. 6 shows the ERS–ENVISAT interferometry DEM over this area. In the eighteenth century this area was still regularly flooded. Then several river corrections were undertaken. The Seeland is characterized by very fertile soils and intensive agriculture. In the case of particularly heavy rains there is still some occasional flooding with immense damage to the agricultural production. The DEM was only derived for the flatter parts. For the more hilly parts phase unwrapping could not reliably be solved because of the very high height sensitivity of the interferometric phase for pairs with such long baselines.

4.2. Potential of cross-interferometry DEMs

To confirm the potential of cross-interferometry DEMs to identify weak small scale topographic features, the DEMs shown in the previous section were compared to the SRTM 3-arc-seconds DEM.

To highlight the sensitivity of the cross-interferometry technique and to better visualize differences to the SRTM DEM Fig. 7 shows the DEMs for a smaller area at the Po Delta. Large portion of these territories lie below the mean sea level and are characterized by a very low degree of urbanization and significant subsidence rates up to 15 mm/year (Teatini et al., 2005, 2007). Tectonics and residual consolidation of clayey deposits contribute to the subsidence general trend, but more local factors, such as peat oxidation, enhanced in turn by agricultural practices, natural compaction of fine-grained deposits in recently reclaimed lagoon sectors and geostatic load increase because of the continuous progradation of the Po river delta, can play a significant role. At present, a large part of the area is kept dry by a distributed drainage system that collects the water from a network of ditches, and pumps it into the sea. The SRTM DEM was oversampled to the same spatial resolution as the ERS–ENVISAT interferometry DEM. Overall there is a good correspondence between the two DEMs. The ERS–ENVISAT interferometry DEM appears significantly less noisy than the SRTM DEM. Careful consideration confirms this and reveals that fine structures are clearly better visible in the ERS–ENVISAT interferometry DEM. The detailed height features observed in the ERS–ENVISAT interferometry DEM correlate well with known morphological features. A major disadvantage of the ERS–ENVISAT interferometry DEM is the missing coverage in areas of temporal decorrelation (such as observed over water) and geometric

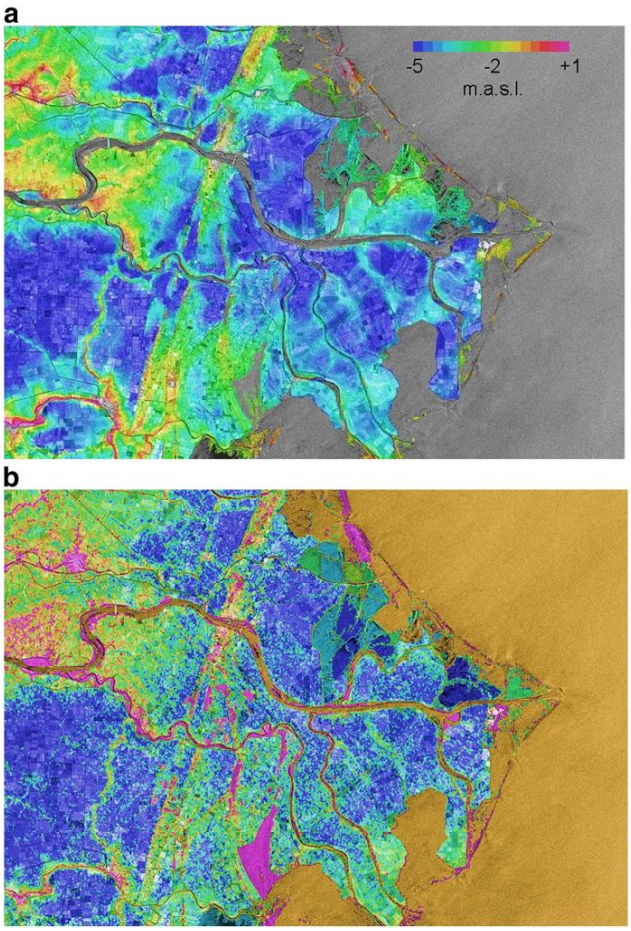


Fig. 7. Comparison of DEMs for 50 km × 35 km area at Po river delta, Italy. The DEM shown in image a is derived using ERS–ENVISAT interferometry (7-Nov-2007, dt 28′, $B_\perp$ 2002 m, dDC 817 Hz). Image b shows the interpolated SRTM-3″ DEM heights over the same area using the identical very fine color scale. In the SRTM DEM areas with forest and buildings are in pink color indicating heights equal to or larger than +1 m.a.s.l.

Author's personal copy

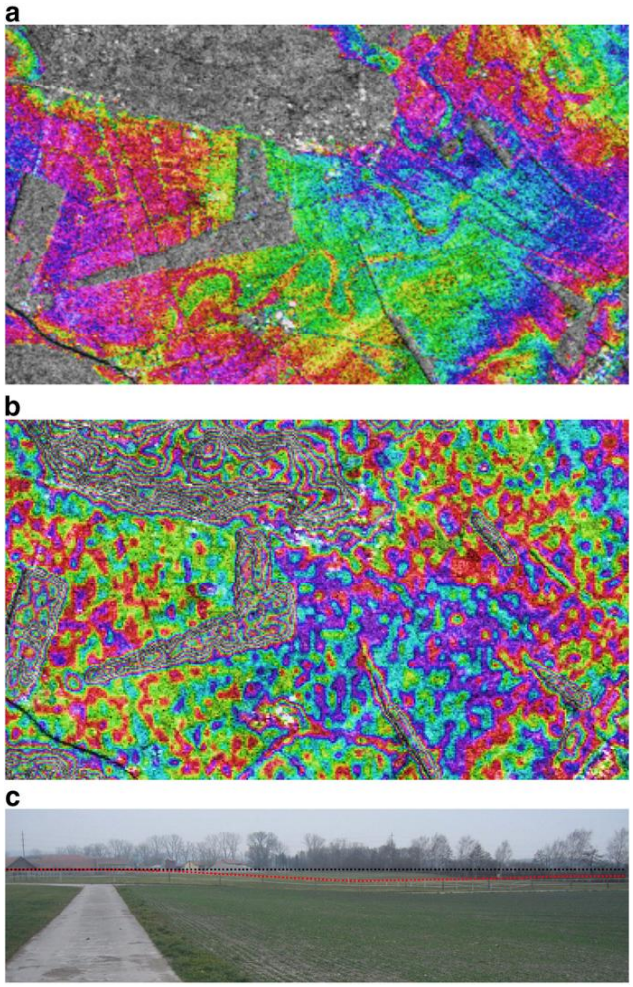


Fig. 8. Identification and mapping of old river beds in the Seeland, Switzerland, becomes possible using the ERS–ENVISAT interferometry DEM (15-Oct-2007, dt 28′, $B_\perp$ 1890 m, dD 237 Hz) shown in the left image. Due to its lower spatial resolution and higher noise the river beds are not clearly visible in the corresponding SRTM DEM shown in the right image. The photograph shows the old river bed marked in the cross-interferometry DEM with a white bar, confirming the 1–2 m height differences identified along this profile. The DEM size is 7.6 km×4.4 km. A cyclic color scale with only 4 m height per color cycle is used to highlight local height variations.

decorrelation (as observed for forest and urban areas, and in the case of sloped terrain because of non-overlapping range reflectivity spectra).

Comparison of the ERS–ENVISAT interferometry DEM over the Seeland site with the SRTM DEM confirms the indications for the Po River Delta. The ERS–ENVISAT interferometry has a significantly higher sensitivity than SRTM and consequently fine structures are better visible. When displayed using a fine color scale the ERS–ENVISAT interferometry DEM section clearly shows some "worm-like" structures not visible in the SRTM DEM (see Fig. 8). Investigating these 1–2 m height changes in more detail showed that they correspond to ancient river beds. Before the river corrections the rivers were obviously strongly meandering in this flat terrain. On the ground the presence of these height changes could be validated. The photograph shown in Fig. 8 confirms the presence of such a height change at one location. The difference between the black horizontal line and the red surface parallel line drawn along a fence is slightly larger than fence height, confirming

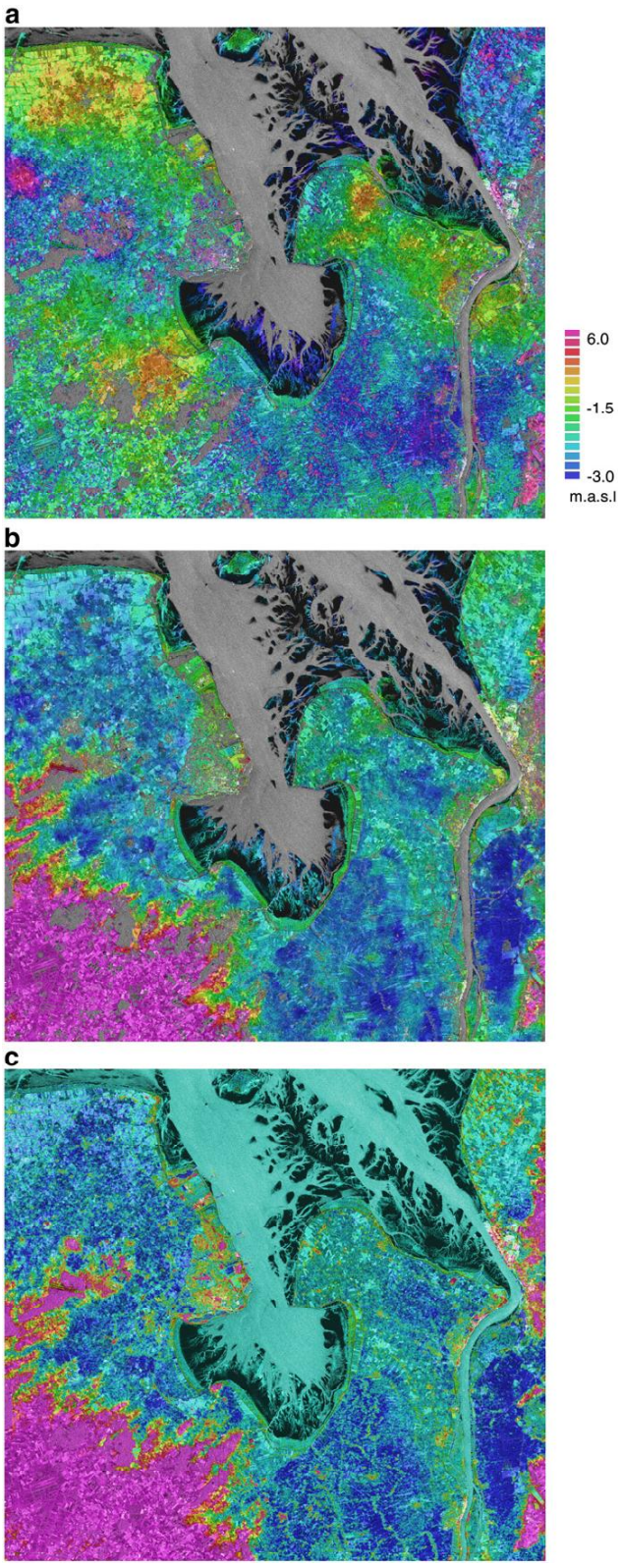


Fig. 9. The images shown are for a 54 km×50 km area around over Wilhelmshaven, Germany. The left image shows the height difference between the ERS–ENVISAT interferometry height (18-Oct-2007, dt 28′, $B_\perp$ 2021 m, dDC 391 Hz) and the interpolated SRTM height, using a color scale between −5 m (pink) and +5 m (orange). The center image shows the "atmosphere corrected" ERS–ENVISAT interferometry DEM and the right image the interpolated SRTM DEM, all using the same color scale between −3 m and +6 m (pink).

Author's personal copy

the 1–2 m identified in the ERS–ENVISAT interferometry DEM. The comparison with the SRTM DEM shows that such local features are much better visible in the cross-interferometry DEM. On the other hand the completeness of the SRTM DEM is significantly better, especially in sloped terrain as well as in forested area and over water.

To highlight the sensitivity of the technique to small height variations over East Frisia, Fig. 9 shows for a 54 km×50 km area the height difference to the SRTM DEM using a fine height scale. A low frequency difference of up to few meters becomes obvious. This difference relates most likely to atmospheric distortions in the ERS–ENVISAT interferometry DEM. Estimating this low frequency offset by strong spatial filtering of the height difference image and subtracting this offset resulted in the "atmosphere corrected DEM" also shown in Fig. 9 together with the SRTM DEM. Again the good sensitivity and low noise of the ERS–ENVISAT interferometry DEM is confirmed. Nevertheless, the potential influence of atmospheric path delay heterogeneity has to be kept in mind. Locally, very strong distortions may cause in more extreme cases height errors of up to 10 m.

5. Conclusions and outlook

After an overview on the ERS–ENVISAT interferometry methodology examples of DEMs derived using ERS-2–ENVISAT ASAR IS2 VV-polarization pairs acquired during the recent dedicated ERS-2–ENVISAT Tandem mission were shown. Pairs with 28 min repeat intervals and 2 km baselines are of interest for DEM generation in relatively flat areas because of the high phase to height sensitivity with ambiguity heights around 5 m. The results very clearly demonstrate the feasibility of this methodology. In all the cases shown, not just differential interferograms were derived, but terrain heights in cartographic projections. In areas of relatively flat terrain, it was possible to process large areas such as demonstrated with the 100 km×300 km area processed over the Western Coast of the Netherlands.

Where DEM values were retrieved, the ERS–ENVISAT interferometry heights were of generally high quality. However, the DEM coverage achieved was not complete. Decorrelation prevented the application of the technique over water, forests, and some urban areas. Apart from the atmospheric error an accuracy of 0.13 m is expected at a coherence level of 0.5. At the large scale the results were compared to SRTM heights. The quality of the SRTM is not sufficient for a quantitative validation of the ERS–ENVISAT interferometry DEMs, therefore the DEMs presented were not yet rigorously validated. Related work should be addressed in the future. For relatively flat agricultural areas the correspondence with the SRTM heights is very good with typical standard deviations below 2 m. This is significantly better than the 6.2 m accuracy reported for the SRTM heights, which is consistent with investigations of Joon and Schwartz (2008) who also found SRTM errors in this range for low relief areas. At more local scale the ERS–ENVISAT interferometry heights show finer details than the SRTM DEM and they are less noisy. From this we conclude a high potential for elevation mapping in coastal studies, lowlands, floodplains, wetlands and other rather flat areas. This potential is of particular interest in areas with temporal changes to the relief such as the Wadden Sea area.

From ESA's dedicated ERS-2–ENVISAT Tandem mission between 27 September 2007 and 12 February 2008 many suited pairs with approximately 2 km baselines and sufficient Doppler spectra overlap were acquired over mid and high northern latitudes. Accordingly, the methodology is applicable not just at the sites already demonstrated but much more widely. ESA may also consider similar Tandem operation of ERS-2 and ENVISAT ASAR over other regions.

Acknowledgements

This work was supported by ESA under contract 19366/05/I-EC–CCN5 and the project "ERS-ENVISAT Tandem Cross-InSAR Campaigns: Case Studies". ERS and ENVISAT data are copyright ESA and were received through CAT1 AO Project 4901.

References

Arnaud, A., Adam, N., Hanssen, R., Inglada, J., Duro, J., Closa, J., Eineder, M., 2003. ASAR ERS interferometric phase continuity. Proc. IGARSS'03, Toulouse, 21–25 July.

Bamler, R., Hartl, P., 1998. Synthetic aperture radar interferometry. Inverse Problems, vol. no. 14, pp. R1–R54.

Colesanti, C., De Zan, F., Ferretti, A., Prati, C., Rocca, F., 2003. Generation of DEM with submetric vertical accuracy from 30′ ERS–ENVISAT pairs. Proc. 'Fringe 03' Workshop on ERS SAR and ASAR Interferometry. ESA-ESRIN, Frascati. 1–5 December.

Hong, S.-H., Won, J.-S., 2005. ERS–ENVISAT cross-interferometry for coastal DEM construction. Proc. Fringe 2005 Workshop. ESA-ESRIN, Frascati. 28 November–2 December.

Hong, S.-H., Won, J.-S., 2006. Application of ERS–ENVISAT cross-interferometry to coastal DEM reconstruction. Proc. EUSAR 2006, Dresden, 16–18 May.

Gatelli, F., Monti Guarnieri, A., Parizzi, F., Pasquali, P., Prati, C., Rocca, F., 1994. The Wavenumber Shift in SAR Interferometry. IEEE Trans. Geosci. Remote Sensing, vol. 32, pp. 855–865.

Joon, K., Schwartz, F., 2008. Limitations in the hydrologic applications of C-band SRTM DEMs in low-relief settings. Geoscience and Remote Sensing Letters 5 (3), 497–501.

Meadows P.J., Rosich, B., Pilgrim, A., Tranfaglia, M.,2007. ERS-2 SAR Performance and Product Evolution, Proc. Envisat Symposium 2007, Montreux, Switzerland, 23–27 April 2007 (ESA publication SP-636).

Miranda N., Rosich, B., Santella, C., 2004. Review of the Impact of the ERS-2 Piloting Modes on the SAR Doppler Stability", Envisat & ERS Symposium, Salzburg, Austria, 6–10 September 2004 (ESA publication SP-572).

Monti Guarnieri, A., Prati, C., 2000. ERS–ENVISAT combination for interferometry and super-resolution. Proc. ERS–Envisat Symposium, Gothenburg, 16–20 October.

Rabus, B., Eineder, M., Roth, A., Bamler, R., 2003. The shuttle radar topography mission — a new class of digital elevation models acquired by spaceborne radar. ISPRS Journal of Photogrammetry and Remote Sensing 57 (4), 241–262.

Rodríguez, E., Martin, J.M., 1992. Theory and design of interferometric synthetic-aperture radars. Proceedings of the Institution of Electrical Engineers 139 (2), 147–159.

Rodríguez, E., Morris, C., Belz, J., 2006. A Global Assessment of the SRTM Performance. Photogrammetric Engineering and Remote Sensing 72 (3), 249–260.

Rosen, P., Hensley, S., Joughin, I., Li, F., Madsen, S., Rodriguez, E., Goldstein, R., 2000. Synthetic aperture radar interferometry. Proceedings of the IEEE 88 (3), 333–382 March.

Santoro, M., Askne, J.I.H., Wegmüller, U., Werner, C.L., 2007. Observations, modeling, and applications of ERS–ENVISAT coherence over land surfaces. IEEE Transactions on Geoscience and Remote Sensing 45 (8), 2600–2611.

Teatini, P., Tosi, L., Strozzi, T., Carbognin, L., Wegmüller, U., Rizzetto, F., 2005. Mapping Regional Land Displacements in the Venice Coastland by an Integrated Monitoring System. Remote Sensing of Environment, vol. 98, pp. 403–413. doi:10.1016/j.rse.2005.08.002.

Teatini, P., Strozzi, T., Tosi, L., Wegmueller, U., Werner, C., Carbognin, L., 2007. Assessing short- and long-time displacements in the Venice coastland by synthetic aperture radar interferometric point target analysis. Journal of Geophysical Research 112, F01012. doi:10.1029/2006JF000656.

Wegmüller, U., Werner, C., Strozzi, T., Wiesmann, A., 2005. ERS–ASAR integration in the interferometric point target analysis. Proc. Fringe 2005 Workshop. ESA-ESRIN, Frascati. 28 November–2 December.